The EPR Signals from the S_0 and S_2 States of the Mn Cluster in Photosystem II Relax Differently†

Sindra Peterson, Karin A. Åhrling,‡ and Stenbjörn Styring*

Department of Biochemistry, Center for Chemistry and Chemical Engineering, Lund University, P.O. Box 124, S-221 00 Lund, Sweden

Received March 1, 1999; Revised Manuscript Received September 9, 1999

ABSTRACT: The oxygen evolving complex (OEC) of photosystem II (PSII) gives rise to manganese-derived electron paramagnetic resonance (EPR) signals in the S_0 and S_2 oxidation states. These signals exhibit different microwave power saturation behavior between 4 and 10 K. Below 8 K, the S_0 state EPR signal is a faster relaxer than the S_2 multiline signal, but above 8 K, the S_0 signal is the slower relaxer of the two. The different temperature dependencies of the relaxation of the S_0 and S_2 ground-state Mn signals are due to differences in the spin−lattice relaxation process. The dominating spin−lattice relaxation mechanism is concluded to be a Raman mechanism in the S_0 state, with a $T^{4.1}$ temperature dependence of the relaxation rate. It is proposed that the relaxation of the S_2 state arises from a Raman mechanism as well, with a $T^{6.8}$ temperature dependence of the relaxation rate, although the data also fit an Orbach process. If both signals relax through a Raman mechanism, the different exponents are proposed to reflect structural differences in the proteins surrounding the Mn cluster between the S_0 and S_2 states. The saturation of SII_{slow} from the Y_D^{ox} radical on the D2 protein was also studied, and found to vary between the S_0 and the S_2 states of the enzyme in a manner similar to the EPR signals from the OEC. Furthermore, we found that the S_2 multiline signal in the second turnover of the enzyme is significantly more difficult to saturate than in the first turnover. This suggests differences in the OEC between the first and second cycles of the enzyme. The increased relaxation rate may be caused by the appearance of a relaxation enhancer, or it may be due to subtle structural changes as the OEC is brought into an active state.

Photosystem II (PSII)[1] catalyzes the light-driven oxidation of water to molecular oxygen in the chloroplasts of higher plants. The site for this process, the oxygen evolving complex (OEC), contains four Mn atoms, probably arranged as two di-μ-oxo-bridged dimers (*1*−*4*). Upon illumination, the PSII reaction center pigment P680 is oxidized, and immediately rereduced by a nearby tyrosyl residue, Y_Z, on the D1 reaction center protein (*5*, *6*). Y_Z in turn extracts electrons [or hydrogen atoms (*7*)] from the OEC, causing it to cycle through the five oxidation states S_0−S_4 (*8*), and oxidize water to oxygen. The one-electron oxidation steps $S_0 \rightarrow S_1$, $S_1 \rightarrow S_2$, $S_2 \rightarrow S_3$, and $S_3 \rightarrow S_4$ are light-induced, while $S_4 \rightarrow S_0$ represents the actual evolution of O_2, and occurs spontaneously after the $S_3 \rightarrow S_4$ transition. The most stable state of the OEC is S_1; a dark-adapted PSII sample has 75% of the PSII centers in S_1, and the rest in S_0. This complicates studies of the individual S states, since advancement through the S cycle by flashes will result in samples with mixtures of several S states. This can be avoided with a preflash treatment, described in ref *18*, which yields samples with close to 100% S_1 as starting material. By giving a preflashed, synchronized sample consecutive short flashes of light, the S cycle can be studied step by step.

Electron paramagnetic resonance (EPR) is a powerful method to monitor the electron-transfer processes of PSII. The S_0 and S_2 states are paramagnetic, each giving rise to a broad, fine-structured Mn EPR signal centered around $g = 2$. Since the so-called S_2 multiline EPR signal was discovered in 1981 (*9*), extensive experimental and theoretical investigations have shown that the spectrum arises from an $S = 1/2$ ground state of the Mn cluster with Mn oxidation states $III-IV_3$ or $IV-III_3$. The spectrum has been simulated in terms of an antiferromagnetically coupled mixed valence dimer, affected by the other Mn ions and a His ligand (*10*), and in terms of a tightly coupled Mn tetramer, where all the Mn contribute to the spectral shape (*11*−*13*). The cluster can be viewed as being composed of a 'redox-active' and a 'redox-inactive' pair, where two of the Mn change valence through the S cycle, and two do not (*3*).

The S_0 EPR signal was discovered in 1997 (*14*−*16*), and only appears in the presence of a few percent of methanol, an addition that does not inhibit the oxygen evolving capacity of the centers. The S_0 EPR signal is at least 2800 G wide (*17*), and has lower amplitude and different peak spacing than the S_2 multiline signal. It appears to arise from a $Mn^{II}-Mn^{III}$ state of the redox active pair, in a thermally isolated $S = 1/2$ ground state (*17*).

† This work was supported by the Swedish National Science Research Council, the Knut and Alice Wallenberg Foundation, and the Crafoord Foundation.

‡ Present address: Photobioenergetics Unit, Research School of Biological Sciences, The Institute of Advanced Studies, Australian National University, Canberra 0200, Australia.

[1] Abbreviations: PSII, photosystem II; OEC, oxygen evolving complex; RC, reaction center; EPR, electron paramagnetic resonance; cw EPR, continuous wave EPR; Y_Z, tyrosine Z; Y_D, tyrosine D; SII_{slow}, signal II_{slow}.

10.1021/bi990474e CCC: $18.00
Published on Web 10/27/1999

There is a second redox active tyrosyl residue on the donor side of PSII, denoted Y_D. Y_D is situated on the D2 protein and does not participate in the continuous electron-transport chain. The first photoexcitation of a PSII sample that has been dark-adapted for 1−2 h oxidizes Y_D, resulting in the very stable Y_D^{ox} radical, which gives rise to the EPR signal II_{slow} (SII_{slow}). The presence of a stable radical on the donor side of PSII provides a useful spectroscopic probe, and studies of SII_{slow} have provided much information on the structure and function of the redox components located there. In particular, distance and redox information on various components of PSII has been obtained through saturation studies of the Y_D^{ox} radical (*18*−*21*).

In this work, we seek information about the S_0 state of the oxygen evolving cycle through saturation studies of the EPR signal from S_0. For comparison, similar studies have been carried out in the S_2 state, in methanol-containing samples. To further expand the picture, the saturation behavior of SII_{slow}, which is affected by the redox state of the metal center of the OEC, has been monitored in the same samples in the two S states.

EXPERIMENTAL PROCEDURES

Sample Preparation. PSII-enriched membranes were prepared in dim green light as described by Pace et al. (*22*). EPR samples were prepared with 3% v/v methanol and 10 mM phenyl-*p*-benzoquinone (PpBQ) directly in EPR tubes, at a concentration of 4.5 mg of Chl/mL. This methanol concentration modifies and enhances the EPR signals from S_0 and S_2 fully, without inhibiting oxygen evolution (*23*). A preflash treatment was used to synchronize the centers (*14*, *18*), followed by an appropriate number of flashes at room temperature to enrich the S_2 state (one or five flashes) or the S_0 state (three flashes). The samples were frozen within 1 s in a solid CO_2−ethanol bath, and then rapidly transferred to liquid nitrogen. The flashes were delivered by a Nd:YAG laser (532 nm, 7 ns, 400 mJ/pulse) at a time interval of 0.5−1 s. The S state distribution of each sample is established by monitoring the amplitude of the S_2 multiline signal as a function of the number of flashes given to the samples. From this oscillation pattern, the amount of misses per flash and the S state distribution are calculated (*14*, *18*). Our samples yield a multiline oscillation that can be fit with 100% S_1 in the preflashed sample, and 15% misses per flash after that, yielding 85% S_2 (15% S_1) after one flash, 61% S_0 (6% S_2, 33% S_3) after three flashes, and 45% S_2 (40% S_1, 15% S_0) after five flashes (data not shown).

EPR Spectroscopy and Data Handling. Cw EPR spectra were recorded with a Bruker ESP380 spectrometer (microwave power range: 0−360 mW) equipped with an Oxford Instruments cryostat and temperature controller. The multiline signals from S_0 and S_2 were quantified by the amplitude of characteristic hyperfine peaks, as indicated in Figure 1. The peaks used for the S_0 analysis are chosen to minimize contributions from any S_2 multiline signal remaining after the three flashes (<10% of the centers). For the S_2 multiline, the choice of peaks is less crucial, as these samples, given one flash, are free from S_0. Pace et al. (*22*) have shown that the edge peaks of the S_2 multiline saturate more readily than the central parts of the spectrum. The peaks used in our analysis belong to the central region of the S_2 multiline signal. To investigate whether there are similar variations across the S_0 spectrum, we attempted an analysis of the saturation behavior of the S_0 signal at 7 K from two alternative, more central, peaks, indicated with asterisks in Figure 1. The S_2 peaks are pronounced in this area, but shifted from the S_0 peaks, making the analysis possible. In the case of the S_0 signal, the $P_{1/2}$ values obtained from the edge and central peak selections respectively differed with only a few percent (data not shown). We conclude that the validity of our analysis is not restricted by the peak selection.

SII_{slow} was detected with a modulation frequency of 12.5 kHz to avoid the rapid passage effects on this signal at higher frequencies. To ensure accuracy of the temperature measurements, the temperature dependence of the heme of myoglobin and the $g = 4$ rhombic iron signal of PSII were recorded, and compared to the results of other investigations. The results were satisfactory, with a maximum deviation of 0.3 K over the studied temperature interval. (For further details, see ref *17*.) Data handling of the EPR spectra was carried out with the Bruker WinEPR software.

Analysis of Y_D^{ox} Saturation in Each S State. SII_{slow} from Y_D^{ox} is visible in all S states, and has a different relaxation behavior in each (*18*). Thus, a measured saturation curve represents the S state mix of the sample (see above). Therefore, the data from a flashed sample were deconvoluted so as to represent a pure S state prior to saturation analysis. This was done successively from the zero-flash sample and up, using the known S state distribution, as described by Styring and Rutherford (*18*).

Once deconvoluted, the data are plotted according to eq 5 (see below). Galli et al. (*24*) have discovered that there is some ambiguity in a fit to eq 5, due to dipolar contributions to SII_{slow} saturation. They report that the orientation dependence of the dipolar interactions creates a spread in the detected $P_{1/2}$ value, resulting in a softer bend in the plots in Figure 4 than predicted by eq 5. However, the unsaturated and fully saturated regions of the plot are unaffected by this. To avoid the dipolar contributions to the curved region, we extrapolated $P_{1/2}$ from the linear regions, as described under Results. Despite the orientation-dependent spread of the $P_{1/2}$ values in a sample, the $P_{1/2}$ value obtained by such an extrapolation is specific for the S state and temperature.

RESULTS

Microwave Power Saturation of the S_0 and S_2 Signals. The saturation behavior of the S_0 and S_2 multiline EPR signals has been studied by progressively increasing the cw microwave power at several temperatures in the range 4−10 K. Figure 1 shows the unsaturated spectra from the two states at 7 K. The triangles indicate the peaks used for amplitude analysis throughout this paper.

Here we have studied how the amplitudes of the two spectra vary with the applied microwave power. The measurements are performed at several temperatures, to extract information on the relaxation processes of the spin systems involved. A selection of the saturation data is displayed in Figure 2A. The saturation behavior of the S_0 (filled symbols) and S_2 (open symbols) signals is shown at 4.2, 6.5, and 8 K.

At 4.2 K, the S_0 signal increases with the root microwave power up to a certain point, after which the curve flattens

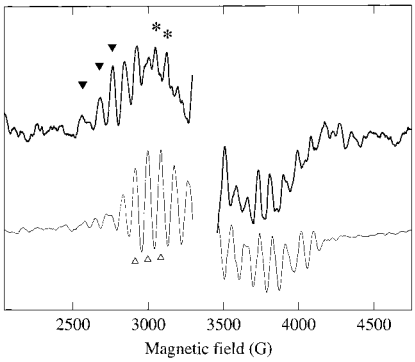

FIGURE 1: The S_0 state EPR signal (boldface) and the S_2 state multiline signal (lightface) recorded at 7 K in samples given three flashes and one flash, respectively. The peaks used for amplitude analysis in this paper are indicated with triangles. The asterisks denote alternative peaks used for S_0 quantitation. The saturated signal from Y_D^{ox} in the middle of the spectra has been removed. EPR settings: microwave frequency, 9.47 GHz; microwave power, 14 mW for S_2, 55 mW for S_0; modulation frequency, 100 kHz; modulation amplitude, 20 G. Note that the spectra shown do not represent the relative amplitudes of the signals; the S_0 signal has been enlarged for clarity.

out and decreases. The power of half-saturation is 10 mW. The S_2 multiline signal has its half-saturation value at a lower power, 1.7 mW, being much more easily saturated than the S_0 signal. The power needed to saturate the Mn signals increases with temperature, but at a different rate for the different signals. Below 8 K, the S_0 signal is more difficult to saturate than the S_2 multiline, but at 8 K the two signals saturate similarly, and at 10 K the S_2 signal is the faster relaxer of the two (Figure 2B).

As the signal-to-noise ratio decreases with increasing temperature, the low peak amplitude of the S_0 signal makes it difficult to obtain data above 10 K. Also, higher microwave intensity than is available with our spectrometer is required to extract reliable saturation information at higher temperatures from the Mn signals, which both are very efficient relaxers.

The microwave power saturation curves (Figure 2A) have been fitted to the equation:

$$I = I_0\sqrt{P/(1 + P/P_{1/2})^b} \qquad (1)$$

where I is the intensity of the signal at power P (in milliwatts), I_0 is the initial slope or unsaturated amplitude of the signal, and $P_{1/2}$ is the microwave power in milliwatts at half-saturation. b has been set to 1, assuming inhomogeneous broadening of the EPR signals (*25*). The observed decrease of signal at high power at 4.2 K indicates that b is greater than 1 at this temperature, but this does not change the estimates of $P_{1/2}$ substantially. The data and fits of Figure 2A have been normalized to $I_0 = 1$, to facilitate comparison of their saturation behavior, as expressed by the single parameter $P_{1/2}$.

Temperature Dependence of $P_{1/2}$. In Figure 2B, the $P_{1/2}$ values obtained from the S_0 and S_2 multiline signals in the temperature range 4−10 K are plotted vs temperature. The two states show different variations of $P_{1/2}$ with temperature, with S_0 being the fastest relaxer below 8 K and S_2 the fastest relaxer above.

The variation of $P_{1/2}$ with temperature is indicative of the nature of the relaxation processes involved. $P_{1/2}$ is a complex

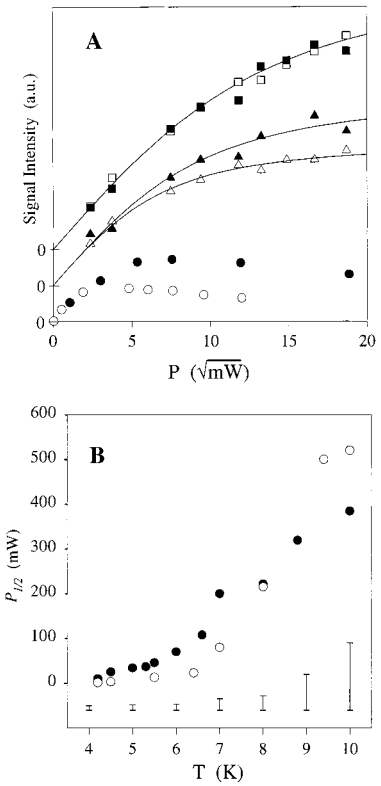

FIGURE 2: (A) EPR signal intensity vs the square root of the microwave power for the S_0 EPR signal (filled symbols) and the S_2 multiline signal (open symbols) measured at 4.2 K (circles), 6.5 K (triangles), and 8 K (squares). All curves have been normalized to the same initial slope (I_0 of eq 1), and the different temperature series have been separated vertically for clarity. The fits to eq 1 (solid lines) represent $P_{1/2}$ values of 110 mW (S_0 6.5 K), 24 mW (S_2 6.5 K), and 220 mW (both signals 8 K). The data taken at 4.2 K were fitted by hand to $P_{1/2} = 10$ mW for S_0 and $P_{1/2} = 1.7$ mW for S_2. All EPR settings were as in Figure 1 except for the microwave power and the temperature, which were varied. (B) $P_{1/2}$ for the S_0 (filled circles) and S_2 (empty circles) state EPR signals vs temperature. The $P_{1/2}$ values were determined from eq 1, as in (A). The error of $P_{1/2}$ determination varies with temperature as indicated. The error bars were estimated from the uncertainty of the fits to eq 1 and the uncertainty of the temperature measurement [±0.3 K (*17*)].

observable, often described by

$$P_{1/2} = \alpha/T_1T_2 \qquad (2)$$

where T_1^{-1} is the spin−lattice relaxation rate, T_2^{-1} is the spin−spin relaxation rate, and α is a constant. T_2 processes involve energy redistribution within the spin system, and T_1 is dependent on the interactions between the paramagnetic center and its surroundings. Pulsed T_1 measurements (*26*) and cw $P_{1/2}$ measurements (*22, 27*−*29*) of the S_2 multiline have given similar results: an exponential fit of the data vs $1/T$ yields approximately the same linear fit. This means that T_2 processes do not contribute significantly to the temperature dependence of $P_{1/2}$ in the S_2 state in the temperature interval covered by these studies.

The very fast relaxation of the S_0 signal makes it difficult to induce a spin−echo above 5 K with our available instrumentation. It has therefore not been possible to study the variation of T_1 over a significant temperature range. Therefore, in analyzing our $P_{1/2}$ data, we assume that what was found for S_2 is applicable to S_0 as well: that T_1 is the

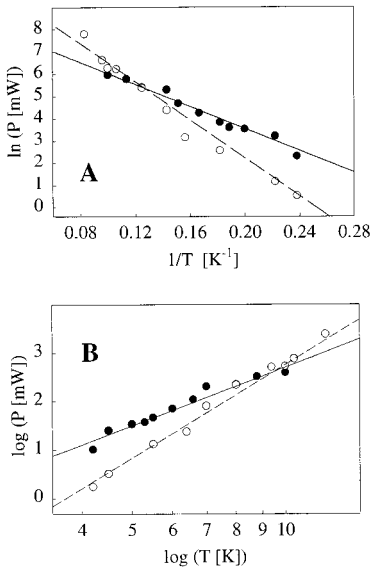

FIGURE 3: (A) Orbach plot of the $P_{1/2}$ data from Figure 2 (eq 3) with fits representing $\Delta = (17 \pm 1)$ cm^{-1} for the S_0 (filled circles) and $\Delta = (30 \pm 2)$ cm^{-1} for the S_2 (open circles) multiline signals from the Mn cluster. (B) Raman plot of the $P_{1/2}$ data from Figure 2 (eq 4) with fits representing $n = 4.1 \pm 0.3$ for S_0 (filled circles) and $n = 6.8 \pm 0.2$ for S_2 (open circles).

main contributor to $P_{1/2}$ over the temperature range studied. Furthermore, the T_1 formalisms employed (*25*, *30*, *31*) fit our data well, implying that T_2 processes do not contribute significantly (*29*).

Relaxation is the release of energy following the EPR microwave absorption. In the case of spin−lattice relaxation, the energy is taken up by the lattice in which the spin system is situated. The spin−lattice relaxation rate, and its temperature dependence, is determined by the mechanism by which the lattice accepts the excess energy.

If the vibrational spectrum of the lattice covers a frequency equivalent to the microwave absorption of the paramagnetic species, a direct relaxation process is possible. This energy gap is small, and the direct process typically dominates at temperatures below 2 K (*30*).

At higher temperatures, where the vibrational spectrum of the lattice spans higher energies, relaxation can instead occur via an excited state of the system. This is called an Orbach process, and involves the absorption of a phonon from the lattice followed by the emission of a phonon of slightly higher energy. The Orbach mechanism gives rise to an exponential temperature dependence of the relaxation rate:

$$1/T_1 \propto e^{-\Delta/k_B T} \qquad (3)$$

where Δ is the energy gap from the ground-state manifold to the excited state, T is the temperature, and k_B is the Bolzmann constant.

Figure 3A shows fits of the data of Figure 2B to eq 3. The fits require Δ values of (30 ± 2) cm^{-1} for S_2, and (17 ± 1) cm^{-1} for S_0.

The third plausible spin−lattice relaxation mechanism is the Raman mechanism, where the spin system is relieved of excess energy through the scattering of a phonon in the surrounding protein lattice. It can be pictured as an Orbach-like process, in which relaxation occurs via a virtual, short-lived higher energy state. The energy of this state is not related to the actual energy levels of the spin system, but determined by the accessible phonon energies in the protein lattice. The probability of such a process taking place is low, but the Raman process gains strength by its ability to utilize a large part of the vibrational spectrum of the lattice. If the ground state is isolated, and there is no accessible excited state, the Raman mechanism will dominate. The Raman relaxation rate varies with temperature as

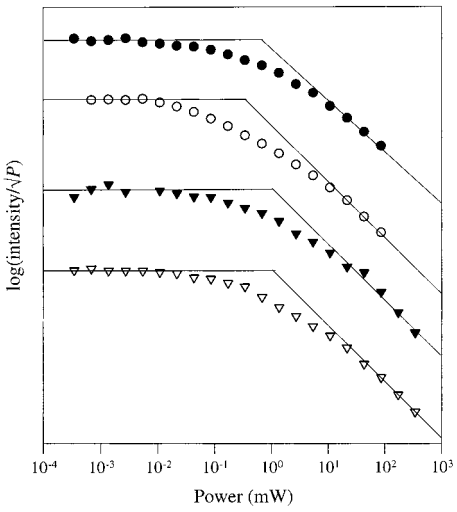

FIGURE 4: Microwave power saturation data from signal II_{slow} from Y_D^{ox} in the S_0 and S_2 states, at 4.3 and 20 K. Filled circles, S_0, 4.3 K; empty circles, S_2, 4.3 K; filled triangles, S_0, 20 K; empty triangles, S_2, 20 K. The signal intensity was taken as the double integral of the EPR signal. EPR settings: modulation frequency, 12.5 kHz; modulation amplitude, 3.16 G; microwave frequency, 9.47 GHz.

$$1/T_1 \propto T^n \qquad (4)$$

where n typically takes on values between 3 and 9 (see Discussion). As shown in Figure 3B, this gives an equally good fit to our data as the Orbach process, with a $T^{(4.1\pm0.3)}$ temperature dependence of the S_0 signal and a $T^{(6.8\pm0.2)}$ temperature dependence of the S_2 signal.

Y_D as a Probe of Manganese Relaxation. Although Y_D takes no active part in the S-cycle, the relaxation behavior of SII_{slow} from Y_D^{ox} varies with the oxidation state of the Mn cluster (*18*). When this was discovered, the S_0 signal was not known. Therefore, the correlation between Y_D^{ox} relaxation and Mn relaxation in different S states could not be fully exploited. We have monitored SII_{slow} relaxation in the S_0 and S_2 samples, and found that it well reflects the behavior of the Mn EPR signals. We have obtained $P_{1/2}$ values of SII_{slow} at temperatures of 4.3 and 20 K; one below and one above the intersection around 8 K found for the relaxation rates of the S_0 and S_2 Mn signals (Figure 2B). Figure 4 shows the microwave power saturation data of SII_{slow}, plotted according to a logarithmic form of eq 1:

$$\log(I/\sqrt{P}) = \log I_0 - b/2 \times \log(1 + P/P_{1/2}) \qquad (5)$$

The data have been deconvoluted from one- and three-flash samples, to represent the pure S_2 and S_0 states, respectively. At unsaturating powers, $\log(I/\sqrt{P})$ is constant, and at high powers, $\log(I/\sqrt{P})$ decreases linearly with log P, with a slope of $b/2$. Extrapolation of these linear regimes gives the apparent $P_{1/2}$ of SII_{slow} at the point of intersection

Table 1: Microwave Power of Half-Saturation ($P_{1/2}$) of the EPR Signals from Y_D^{ox} and the Mn Cluster in the S_0 and S_2 States at Several Temperatures

	Mn signals[a]		SII_{slow}, this work[b]		SII_{slow}, 1988[c]	
	4.2 K	10 K	4.3 K	20 K	8 K	20 K
S_0	10 mW	380 mW	660 μW	1000 μW	155 μW	448 μW
S_2	1.7 mW	520 mW	320 μW	1000 μW	105 μW	790 μW

[a]Data from Figure 2. [b]Deconvoluted $P_{1/2}$ data from measurements of SII_{slow} in PSII-enriched membranes given three flashes (predominantly S_0) or one flash (predominantly S_2), representing the $P_{1/2}$ values of SII_{slow} in the separate S states (Figure 4). [c]Deconvoluted $P_{1/2}$ data of SII_{slow} in the S_0 and S_2 states from Styring and Rutherford (1988) (*18*).

(see Experimental Procedures) (*18*). It is clear that $P_{1/2}$ of SII_{slow} varies both with temperature and with S state. $P_{1/2}$ in the S_2 state clearly occurs at lower microwave power at 4.3 K than at 20 K. The same holds for the S_0 state. SII_{slow} at 4.3 K is a faster relaxer in S_0 than in S_2.

The deconvoluted $P_{1/2}$ values deducted from Figure 4 are listed in Table 1, along with our microwave power saturation results from the manganese EPR signals. Comparable microwave power saturation data from SII_{slow} obtained by Styring and Rutherford in 1988 (*18*) are also listed. At 4.2 K, the S_0 signal from the Mn cluster relaxes 5 times faster than the S_2 multiline. This faster relaxation of the S_0 signal at 4.2 K is reflected by the relaxation of SII_{slow}, which also is a much faster relaxer in S_0 centers than in S_2 centers at 4.3 K. At higher temperatures, this relationship is changed, with Y_D relaxing similarly in the S_0 and S_2 samples. For the Mn signals, the relationship reverses at higher temperatures, with S_2 relaxing faster than S_0 at 10 K. The intersection of the temperature dependencies occurs at around 8 K. SII_{slow} may have the same trend, but with the intersection occurring at a higher temperature, around 20 K. Although not identical in the $P_{1/2}$ values of SII_{slow}, the earlier results of Styring and Rutherford showed the same trend as our data, with SII_{slow} relaxing 50% faster in the S_0 state than in the S_2 state at 8 K, and much slower in the S_0 state than in the S_2 state at 20 K. The different $P_{1/2}$ values for SII_{slow} reported here and earlier (*18*) are more likely to reflect different PSII preparations, buffers, etc. than differences in the OEC. For example, large differences have been reported between thylakoid membranes and PSII-enriched membrane fragments (*18*), although both preparations were highly functional. Several groups have reported $P_{1/2}$ values of SII_{slow} in Mn-depleted PSII or in dark-adapted PSII. Although the reported $P_{1/2}$ values vary, the sensitivity of Y_D^{ox} to the intactness of the Mn cluster or the S state is always similar.

$P_{1/2}$ of the S_2 Multiline Signal Obtained by One and Five Flashes. Figure 5 shows the microwave power saturation of the S_2 multiline signal in a sample that has received one flash and a sample that has received five flashes. Both samples are dominated by the S_2 state, with twice as high S_2 multiline amplitude in the one-flash sample (85% S_2 content) as in the five-flash sample (45% S_2 content), due to the increased mixing of the S state populations. This amplitude difference has been accounted for in Figure 5 by normalizing the initial slopes. Although in the same S state, the two samples saturate very differently with microwave power. It should be pointed out that the S_0 content of the five-flash sample is no more than 14%, and, consequently, the S_0 signal does not contribute to the five-flash S_2 saturation behavior. At 7 K, the multiline signal after one flash is half-saturated at 80 mW, and after five flashes at 350 mW. The five-flash sample exhibits faster relaxation than the one-flash sample throughout the studied temperature range, 4−11 K (data not shown).

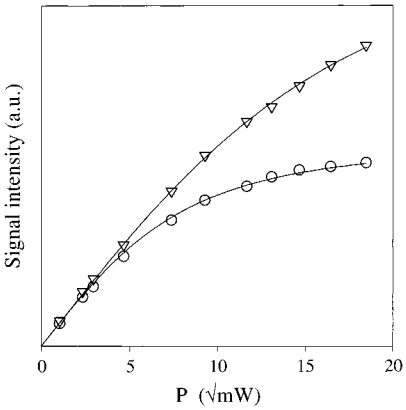

FIGURE 5: Microwave power saturation of the S_2 multiline EPR signal at 7 K in a sample given one flash (circles) and a sample given five flashes (triangles). The two curves have been normalized to the same initial slope for comparison; see text. EPR settings as in Figure 1, except for the microwave power which was varied. The fits represent $P_{1/2} = 80$ mW after one flash, and $P_{1/2} = 350$ mW after five flashes.

The difference between the two samples is the status of the enzyme: the one-flash sample has received a single light-excitation (except for the preflash) after dark-adaptation, while the five-flash sample has passed through one complete S-cycle, and has evolved one molecule of oxygen.

DISCUSSION

Temperature Dependence of $P_{1/2}$ of the S_0 and S_2 Multiline Signals. If an EPR signal relaxes predominantly via an Orbach mechanism, eq 3 holds, and the exponent Δ represents the energy gap between the ground state and the first excited state of the spin system. This gap is determined by the exchange coupling between the Mn ions giving rise to the multiline EPR signal. If the EPR signal arises predominantly from an antiferromagnetically coupled dimer, this coupling constant, $|J|$, can be accurately deducted from the temperature dependence of the unsaturated signal amplitude (I_0 of eq 1), a so-called Curie plot. If all four Mn ions interact strongly to produce the EPR signal, the couplings in the cluster are more complicated, and the $|J|$ deduced from a Curie plot is a resultant of these, rather than a single coupling constant. The resultant $|J|$ is, however, still related to the position of the first excited energy level of the system.

The Orbach analysis of our present relaxation data, shown in Figure 3A, requires a 17 cm^{-1} separation between the ground- and excited-state energy levels of S_0, and a 30 cm^{-1} separation in S_2. This is not in accordance with our comparative study of the Curie plots of both EPR signals (*17*), where we showed that the gap to the first excited state in S_0 is significantly larger than that in S_2. This work excludes an excited state as low as 17 cm^{-1} in the S_0 state. Consequently, an Orbach analysis of the S_0 data (Figure 3A) is not valid. We conclude that the Orbach process is not a dominating contributor to the saturation behavior of the S_0 signal. Instead, relaxation probably occurs via the Raman process.

Our $P_{1/2}$ data from the S_2 state yielded, by the application of an Orbach fit, a 30 cm^{-1} gap between the ground state and an excited state. This is in good accordance with the results of other groups studying the S_2 multiline signal: Hansson et al. and Pace et al. obtained 30 cm^{-1} (*22*, *27*) by $P_{1/2}$ measurements, while Lorigan and Britt obtained 36.5 cm^{-1} by pulsed T_1 measurements (*26*). NH_3-treated PSII centers also yielded 30.5 cm^{-1} (*29*). This asserts the reproducibility of these investigations; the variation of $P_{1/2}$ with temperature seems to be an intrinsic characteristic of the system, and does not vary with preparation procedures or minor additions.

However, the Orbach model usually employed to analyze the data may not be the only feasible interpretation of the S_2 state relaxation behavior. As shown in Figure 3, our data from S_2 can be fitted equally well to a Raman or an Orbach plot.

Although the temperature dependence of $P_{1/2}$ of the S_2 multiline signal is reproducible from lab to lab, the Curie plots obtained by the different groups (*22*, *27*, *28*, *32*, *33*) differ markedly from each other, and from that obtained by us (*17*). This indicates that the magnitude of the exchange interaction in the Mn cluster is sensitive to preparation procedures and sample additions, while the $P_{1/2}$ behavior is not.

This leads us to suggest that the temperature dependence of $P_{1/2}$ in S_2 does not arise from the exchange interaction-dependent Orbach mechanism. The Raman mechanism responsible for the relaxation of the S_0 signal may dominate the S_2 multiline relaxation as well. The Raman temperature dependencies of $P_{1/2}$ of the S_0 and S_2 multiline signals are $T^{4.1}$ and $T^{6.8}$, respectively (Figure 3B).

The Raman relaxation mechanism does not involve the energy levels of the paramagnetic system, but rather depends on the vibrational spectrum of the surrounding lattice. The lattice is the protein holding the Mn cluster, and the delocalized vibrational modes of the protein are determined by its overall structure. This means that the Raman relaxation of the Mn signals involves not only the liganding amino acids, but also more distant parts of the protein environment. The structure of a PSII protein, embedded in the center of the large, multisubunit membrane-bound enzyme complex, is probably less sensitive to external treatment than the energy levels of the more exposed OEC. The Raman mechanism is therefore a feasible explanation of the relaxation behavior found from the S_2 state, reproduced invariantly at the different labs.

Thus, we suggest that the S_0 and the S_2 multiline signals both relax via a Raman mechanism, but with very different Raman exponents. One might wonder if this exponent has any relevant interpretation that will contribute to our understanding of the S-cycle. Stapleton and co-workers have developed a model for iron-containing proteins that correlates the Raman relaxation rate of a paramagnetic center to the backbone structure of the protein holding the paramagnet. If applicable to PSII, this model would indicate structural changes of the protein (or proteins) holding the Mn cluster between the S_0 and the S_2 state.

In Stapleton's work (*34*), an attempt is made to construct a relaxation formalism relevant for biological systems. Traditional solid-state Raman theory predicts odd integer exponents between 3 and 9, specifically T^9 for the Raman relaxation rate of a Kramer's doublet (*31*). In contrast, extensive investigations on cytochromes and iron−sulfur proteins revealed low, noninteger Raman exponents (*35*), suggesting that the relaxation in biological systems is not well described by this theory. Our results from PSII show the same phenomenon, with unexpectedly low Raman exponents. A protein backbone structure model developed in the same group (*34*, *36*) allows a protein to be described by a single fractal parameter, *d*. *d* is a measure of how well a protein fills the Euclidian space it occupies. A low *d* corresponds to a more stretched-out conformation of the protein, a high *d* to a more tightly packed structure. This model was developed for metal-containing proteins (cytochromes), and a relationship was found between *d* and the EPR Raman relaxation rate of the paramagnetic site. *d*, as determined from three-dimensional X-ray structural data, proved successful in predicting the Raman relaxation exponent of the EPR signal from the metal site, with remarkable accuracy.

According to this model, the relaxation rate is affected by the average distance between nonadjacent chain sections of the protein. In other words, changes of secondary structural elements, and changes in the bridging between different groups, would affect the relaxation of the spin system.

Applying this to the data presented here, such differences seem to be present between the S_0 and S_2 states of the OEC. We have found a much weaker temperature dependence of the relaxation rate of the S_0 signal than of the S_2 signal, $T^{4.1}$ and $T^{6.8}$, respectively, suggesting a more compact conformation in S_2. The differences may involve significant rearrangements of the side chains close to the OEC, or secondary structural changes further away. At present, it is not clear which proteins would be involved in such changes, since the Mn cluster may be coordinated to several protein subunits, including the D1 reaction center protein, the CP43 protein, and potentially other proteins in the PSII reaction center. Our conclusions are corroborated by recent FTIR studies of PSII which show changes in the protein structure between the S_1 and S_2 states (*37*−*42*). There could be similar changes in structure between the S_0 and S_1 states, as well.

Concluding, we propose that both the S_0 and S_2 multiline signals relax via the Raman mechanism. The very different Raman exponents found in the two states indicate structural rearrangements in the PSII reaction center between the S_0 and S_2 states.

Stapleton's model was developed for ferric proteins in solution, and may not hold in detail for the Mn cluster region in the PSII reaction center. However, it is not unlikely that the main principle of the model, coupling vibrational relaxation rates to structural changes, is relevant for metal-containing protein systems in general.

If the model is relevant, then our proposal that the protein environment around the Mn cluster changes its overall structure between the S states is of great importance to our understanding of the function of the Mn cluster. For example, such rearrangements could have influence on substrate accessibility, reactivity toward exogenous factors, location of Ca^{2+} and Cl^-, etc. A conclusive determination may have to await high-resolution X-ray structures of the Mn cluster posed in different S states, but until such results are achieved, this kind of analysis is relevant, and complements information from FTIR, CD, and X-ray spectroscopy.

Y_D as a Probe of Manganese Relaxation. The relaxation of SII_{slow} from Y_D^{ox} is enhanced by nearby strongly relaxing paramagnetic centers. The spin−lattice relaxation rate of SII_{slow} has been found to vary with the S state (*18*, *19*) in thylakoid membranes and in PSII-enriched membranes, showing that the Mn cluster acts as such an enhancer. Brudvig and co-workers (*43*) also found that SII_{slow} in Mn-depleted enzymes relaxed differently than model L-tyrosine radicals, and attributed this behavior to relaxation enhancement by the acceptor-side non-heme iron. Thus, the relaxation of SII_{slow} in intact PSII centers may reflect several phenomena in the reaction center. However, S-state-dependent changes must be attributed to interactions with the Mn cluster.

The relaxation rate was found to be slow in the S_1 state, fast in the S_2 and S_3 states, and fastest in the S_0 state (*18*). A very complex temperature dependence of the relaxation was also described (*18*, *19*) in which the S_0 state was the most efficient relaxer of SII_{slow} at low temperature while the S_2 and S_3 states were the more efficient relaxers above 10−15 K. At that time, only the S_2 state EPR signals from the Mn cluster were known. Thus, it was not possible to correlate the relaxation of SII_{slow} directly to that of the Mn cluster. Despite this limitation, important conclusions, which still to a large extent are valid, were drawn about the redox changes in the S-cycle.

Here, we have been able to substantiate the earlier conclusion that SII_{slow} is a sensitive relaxation probe to changes in the Mn cluster in the S-cycle, via direct comparison of SII_{slow} relaxation and relaxation of the Mn signals. At low temperature, the S_0 EPR signal relaxes faster than the S_2 state multiline signal. Above 8 K, the situation is opposite, and the S_2 multiline signal relaxes faster. This behavior is well, although not completely, reflected in the relaxation behavior of the Y_D^{ox} radical (Table 1). Thus, we conclude, similar to what was proposed from biochemical experiments (*44*), that relaxation studies of SII_{slow} in oxygen evolving PSII report mainly on the chemistry in the Mn cluster. However, the disagreement between the relaxation behavior of the Mn signals and SII_{slow} (Table 1) also implies that other, temperature-dependent relaxation mechanisms might contribute to the SII_{slow} relaxation—such as interaction with the non-heme iron (*43*), or influence of oxygen in the site (*45*). Investigation of the separate mechanisms involved is being conducted.

Saturation of the S_2 Multiline Signal after One and Five Flashes. Unexpectedly, we found that the S_2 multiline signal relaxes faster on the second turnover of the enzyme than on the first.

Similar behavior, probably related to our results on the relaxation of the S_2 multiline signal, has been reported for SII_{slow} in the S_1 state. Styring and Rutherford (*18*) found that SII_{slow} in a four-flash sample relaxes twice as efficiently as SII_{slow} in a sample that was only preflashed. They explained it in terms of S_0 contributions in the four-flash sample. However, this was later shown to reflect changes in the S_1 state, and Van Vliet and Rutherford (*45*) demonstrated that the addition of PpBQ diminished the difference in SII_{slow} relaxation between the two S_1 samples.

The direct $P_{1/2}$ measurement on the S_2 multiline signal presented here is not influenced by PSII centers in other S states. Furthermore, all our samples contain PpBQ. Thus, our measurements on the Mn EPR signal strongly suggest that the Mn cluster in the S_2 state changes its relaxation properties during the first turnover of the OEC.

A different relaxation rate could be caused by changes in the Mn cluster itself, or by the buildup of a relaxation enhancer in the immediate vicinity of the Mn cluster. Gross conformational changes may involve an activation of the enzyme during the first turnover after dark-adaption; the concept of a resting state and an active state of PSII has been suggested earlier (*46*). Major changes in the Mn cluster itself seem less likely since the multiline EPR signal, which is a very sensitive probe to the Mn cluster structure, is unchanged (to our present knowledge) between a sample given one flash and a sample given five flashes. The possibility of a relaxation enhancer building up during the first turnover of the enzyme is intriguing, and several candidates can be imagined (including oxygen and reduced PpBQ; compare ref *45*).

ACKNOWLEDGMENT

We acknowledge valuable discussions with Dr. J.-J. Girerd and Dr. R. J. Pace.

REFERENCES

1. Rutherford, A. W. (1989) *Trends Biol. Sci. 14*, 227−232.
2. Debus, R. J. (1992) *Biochim. Biophys. Acta 1102*, 269−352.
3. Yachandra, V. K., Sauer, K., and Klein, M. P. (1996) *Chem. Rev. 96*, 2927−2950.
4. Britt, D. R. (1996) in *Oxygenic Photosynthesis: the Light Reactions* (Ort, D. R., and Yocum, C. F., Eds.) pp 137−164, Kluwer Academic Publishers, Dordrecht.
5. Blankenship, R. E., Babcock, G. T., Warden, J. T., and Sauer, K. (1975) *FEBS Lett. 51*, 287−293.
6. Babcock, G. T., Barry, B. A., Debus, R. J., Hoganson, C. W., Atamian, M., McIntosh, L., Sithole, I., and Yocum, C. F. (1989) *Biochemistry 28*, 9557−9565.
7. Hoganson, C. W., and Babcock, G. T. (1997) *Science 277*, 1953−1956.
8. Kok, B., Forbush, B., and McGloin, M. (1970) *Photochem. Photobiol. 11*, 457−475.
9. Dismukes, G. C., and Siderer, Y. (1981) *Proc. Natl. Acad. Sci. U.S.A. 78*, 274−278.
10. Åhrling, K. A., Smith, P. J., and Pace, R. J. (1998) *J. Am. Chem. Soc. 120*, 13202−13214.
11. Bonvoisin, J., Blondin, G., Girerd, J., and Zimmerman, J. (1992) *Biophys. J. 61*, 1076−1086.
12. Kusunoki, M. (1992) in *Research in Photosynthesis* (Murata, N., Ed.) pp 297−300, Kluwer Academic Publishers, Dordrecht.
13. Zheng, M., and Dismukes, G. C. (1996) *Inorg. Chem. 35*, 3307−3319.
14. Åhrling, K. A., Peterson, S., and Styring, S. (1997) *Biochemistry 36*, 13148−13152.
15. Messinger, J., Nugent, J. H. A., and Evans, M. C. W. (1997) *Biochemistry 36*, 11055−11060.
16. Messinger, J., Robblee, J. H., Yu, W. O., Sauer, K., Yachandra, V. K., and Klein, M. P. (1997) *J. Am. Chem. Soc. 119*, 11349−11350.
17. Åhrling, K. A., Peterson, S., and Styring, S. (1998) *Biochemistry 37*, 8115−8120.
18. Styring, S., and Rutherford, A. W. (1988) *Biochemistry 27*, 4915−4923.
19. Evelo, R. G., Styring, S., Rutherford, A. W., and Hoff, A. J. (1989) *Biochim. Biophys. Acta 973*, 428−442.
20. Beck, W. F., Innes, J. B., and Brudvig, G. W. (1990) in *Current Research in Photosynthesis* (Baltscheffsky, M., Ed.) pp 817−820, Kluwer Academic Publishers, Dordrecht, The Netherlands.
21. Kodera, Y., Takura, K., and Kawamori, A. (1992) *Biochim. Biophys. Acta 1101*, 23−32.

22. Pace, R. J., Smith, P., Bramley, R., and Stehlik, D. (1991) *Biochim. Biophys. Acta 1058*, 161−170.
23. Deák, Z., Peterson, S., Geijer, P., Åhrling, K. A., and Styring, S. (1999) *Biochim. Biophys. Acta 1412*, 240−249.
24. Galli, C., Innes, J. B., Hirsh, D. J., and Brudvig, G. W. (1996) *J. Magn. Reson. B 110*, 284−287.
25. Rupp, H., Rao, K. K., Hall, D. O., and Cammack, R. (1978) *Biochim. Biophys. Acta 537*, 255−269.
26. Lorigan, G. A., and Britt, R. D. (1994) *Biochemistry 33*, 12072−12076.
27. Hansson, Ö., Andreasson, L.-E., and Vänngård, T. (1984) in *Advances in Photosynthesis Research* (Sybesma, C., Ed.) pp 1.3.307−1.3.310, Martinus Nijoff/Dr W. Junk, Hague/Boston/Lancaster.
28. Hansson, O., Aasa, R., and Vänngård, T. (1987) *Biophys. J. 51*, 825−832.
29. Koulougliotis, D., Schweitzer, R. H., and Brudvig, G. W. (1997) *Biochemistry 36*, 9735−9746.
30. Orton, J. W. (1968) *Electron Paramagnetic Resonance—An Introduction to Transition Group Ions in Crystals*, 1st ed., London Iliffe Books Ltd., London.
31. Abragam, A., and Bleany, B. (1970) *Electron Paramagnetic Resonance of Transition Ions*, Dover Publications, Inc., New York.
32. Vänngård, T., and Haddy, A. (1992) in *Manganese Redox Enzymes* (Pecoraro, V. L., Ed.) pp 105−118, VCH, New York.
33. Britt, R. D., Lorigan, G. A., Sauer, K., Klein, M. P., and Zimmerman, J.-L. (1992) *Biochim. Biophys. Acta 1040*, 95−101.
34. Allen, J. P., Colvin, J. T., Stinson, D. G., Flynn, C. P., and Stapleton, H. J. (1982) *Biophys. J. 38*, 299−310.
35. Wagner, G. C., Colvin, J. T., Allen, J. P., and Stapleton, H. J. (1985) *J. Am. Chem. Soc. 107*, 5589−5593.
36. Stapleton, H. P., Allen, J. P., Flynn, C. P., Stinson, D. G., and Kurtz, S. R. (1980) *Phys. Rev. Lett. 45*, 1456−1459.
37. Noguchi, T., Ono, T., and Inoue, Y. (1995) *Biochim. Biophys. Acta 1228*, 189−200.
38. Noguchi, T., Ono, T., and Inoue, Y. (1995) *Biochim. Biophys. Acta 1232*, 59−66.
39. Steenhuis, J. J., and Barry, B. A. (1996) *J. Am. Chem. Soc. 118*, 11927−11932.
40. Steenhuis, J. J., and Barry, B. A. (1997) *J. Phys. Chem. B 101*, 6652−6660.
41. Zhang, H., Razeghifard, M. R., Fischer, G., and Wydrzynski, T. (1997) *Biochemistry 36*, 11762−11768.
42. Chu, H.-A., Gardner, M. T., O'Brien, J. P., Barlow, J., and Babcock, G. T. (1998) in *Photosynthesis: Mechanisms and Effects* (Garab, G., Ed.) pp 1303−1306, Kluwer Academic Publishers, Dordrecht, The Netherlands.
43. Hirsh, D. J., Beck, W. F., Innes, J. B., and Brudvig, G. W. (1992) *Biochemistry 31*, 532−541.
44. Bosch, M. K., Evelo, R. G., Styring, S., Rutherford, A. W., and Hoff, A. J. (1991) *FEBS Lett. 292*, 279−283.
45. Van Vliet, P. (1996) Thesis, Agricultural University, Wageningen, The Netherlands.
46. Beck, W. F., de Paula, J. C., and Brudvig, G. W. (1985) *Biochemistry 24*, 3035−3043.

BI990474E